

## Shedding Light on the Dark Corners of MOF Thin Films: Growth and Structural Stability of ZIF-8 Layers Probed by Optical Waveguide Spectroscopy

Juan Alejandro Allegretto, Jakub Dostalek, Matías Rafti,  
Bernhard Menges, Omar Azzaroni, and Wolfgang Knoll

*J. Phys. Chem. A*, **Just Accepted Manuscript** • DOI: 10.1021/acs.jpca.8b09610 • Publication Date (Web): 19 Nov 2018

Downloaded from <http://pubs.acs.org> on November 22, 2018

### Just Accepted

“Just Accepted” manuscripts have been peer-reviewed and accepted for publication. They are posted online prior to technical editing, formatting for publication and author proofing. The American Chemical Society provides “Just Accepted” as a service to the research community to expedite the dissemination of scientific material as soon as possible after acceptance. “Just Accepted” manuscripts appear in full in PDF format accompanied by an HTML abstract. “Just Accepted” manuscripts have been fully peer reviewed, but should not be considered the official version of record. They are citable by the Digital Object Identifier (DOI®). “Just Accepted” is an optional service offered to authors. Therefore, the “Just Accepted” Web site may not include all articles that will be published in the journal. After a manuscript is technically edited and formatted, it will be removed from the “Just Accepted” Web site and published as an ASAP article. Note that technical editing may introduce minor changes to the manuscript text and/or graphics which could affect content, and all legal disclaimers and ethical guidelines that apply to the journal pertain. ACS cannot be held responsible for errors or consequences arising from the use of information contained in these “Just Accepted” manuscripts.



1  
2  
3  
4  
5  
6  
7 Shedding Light on the Dark Corners of MOF Thin  
8  
9  
10  
11 Films: Growth and Structural Stability of ZIF-8  
12  
13  
14  
15 Layers Probed by Optical Waveguide Spectroscopy  
16  
17  
18  
19

20 Juan A. Allegretto<sup>1,2</sup>, Jakub Dostalek<sup>3</sup>, Matías Rafti<sup>1</sup>, Bernhard Menges<sup>4</sup>, Omar Azzaroni<sup>1\*</sup> and  
21  
22 Wolfgang Knoll<sup>5,6</sup>

23  
24  
25  
26 \*azzaroni@inifta.unlp.edu.ar  
27

28  
29 <sup>1</sup>Instituto de Investigaciones Fisicoquímicas Teóricas y Aplicadas (INIFTA), Departamento de  
30  
31 Química, Facultad de Ciencias Exactas, Universidad Nacional de La Plata, CONICET, Calle 64  
32  
33 y Diag. 113, 1900 La Plata, Argentina.  
34  
35

36  
37 <sup>2</sup>Universidad Nacional de San Martín (UNSAM), San Martín, Argentina.  
38  
39

40 <sup>3</sup>Biosensor Technologies, AIT-Austrian Institute of Technology GmbH, Konrad-Lorenz-Strasse  
41  
42 24, 3430 Tulln, Austria.  
43  
44

45  
46 <sup>4</sup>Resonant Technologies GmbH, Bahnhofstraße 70, 55234 Framersheim, Germany  
47  
48

49 <sup>5</sup>Competence Center for Electrochemical Surface Technology, Konrad Lorenz Strasse 24, 3430  
50  
51 Tulln, Austria.  
52  
53

54  
55 <sup>6</sup>AIT Austrian Institute of Technology, Giefinggasse 4, 1210 Vienna, Austria.  
56  
57  
58  
59  
60

## Abstract

Due to its many features and possible applications, metal-organic frameworks have attracted increasing attention in recent years. Within this type of materials, hydrophobic zeolitic imidazolate framework constituted of  $Zn^{2+}$  metal centers, coordinated by 2-methylimidazolate organic linkers (ZIF-8); has proved to be a highly versatile porous support compatible with diverse applications ranging from sensing platforms to electronics or energy-related devices. However, the study of a crucial parameter such as their structural stability towards exposure to different aqueous environments (relevant for a wide range of applications), remains only partially addressed and constitutes one of the main goals of the present work. By synthesizing mono- and multimode ZIF-8 optical waveguides for both optical waveguide and surface plasmon resonance spectroscopy, it was possible to characterize the ZIF-8 film growth, and its stability in different sensor-relevant liquid environments. Additionally, characterization of polyelectrolyte-modified films was explored, as it constitutes a relevant strategy in order to confer differential properties and enhanced stability to the films.

## Introduction

Metal Organic Frameworks (MOFs)<sup>1,2</sup> can be defined as infinite porous coordination networks constituted by non-covalently linked organic and inorganic units, and offer numerous attractive properties including high surface area, chemical versatility and relatively high chemical and thermal stability. Owing to these features, MOFs have been used to pursue a wide range of applications; to name a few, gas sensors,<sup>3</sup> adsorbents for liquid and gas phase separations,<sup>4</sup> supports for drug-delivery systems,<sup>5</sup> or as separation membranes.<sup>6</sup> Moreover, the facile synthesis methods, and versatility regarding structural and surface chemistry fine-tuning via either pre or post-synthetic procedures<sup>7,8</sup> adds additional appeal to the integration of MOFs in catalytic and adsorption related mixed platforms.<sup>9-11</sup> This relatively new class of materials can be used to prepare films using different strategies depending on the targeted application; e.g., direct spin-coating using colloidal dispersions of nano/microcrystals generate thick and eminently non-smooth films, while surface mounted MOF quasi-monolayer thin films (SURMOFs), allow for the observation of non-bulk physical and chemical properties.<sup>12-14</sup> SURMOFs can be synthesized via the Langmuir-Blodgett method, or directly on top of substrates exposing suitable moieties which would act as primers for growth enhancement. It was also previously demonstrated, that post-synthetic modification of porous films (not only for MOF growth but in general; e.g., mesoporous silica) using polyelectrolytes, can yield a pH-responsive material, or to allow modulation of polar character.<sup>15-19</sup>

An extensively used MOF is the so-called ZIF-8 (Zeolitic Imidazolate Framework, available commercially as BASF-BASOLITE-Z1200<sup>®</sup>); and features a sodalite-like crystalline microporous network based on Zn<sup>2+</sup> clusters tetrahedrally coordinated by 2-methylimidazolate ions (mIm<sup>-</sup>). ZIF-8 was successfully employed for separations,<sup>20-22</sup> in mixed membranes,<sup>23-25</sup> and

1  
2  
3 even for the synthesis of hybrid membranes.<sup>26–29</sup> There are many different strategies for  
4 synthesizing ZIF-8 films, but the hydro/solvothermal method remains the most popular, both in  
5 terms of simplicity and reproducibility. One of the areas in which the use of MOFs in general,  
6 and ZIF-8, in particular, is gaining increasing interest is sensor technologies,<sup>30–32</sup> which takes  
7 advantage of its high microporosity and surface area. A recent example of ZIF-8 films use for  
8 sensing applications is the work of Lu and Hupp,<sup>33</sup> in which the authors took advantage of the  
9 effect of different adsorbed analytes on the Fabry-Pérot interference phenomena (which gives  
10 rise to different colors) in order to detect such chemicals via UV-vis transmission spectroscopy.  
11 Propane, ethanol, water and water/ethanol mixtures were used taking in consideration the  
12 hydrophobicity of ZIF-8 micropores. In a similar fashion, Li *et al.* presented a photonic crystal  
13 fabricated with a structured ZIF-8 thin layer with narrow spectral resonances.<sup>34</sup> Time-resolved  
14 reflectometry performed on this material allowed for the monitoring of acetonitrile adsorption in  
15 the ZIF-8 layer. Another possible strategy is to probe the interaction between analyte and MOF  
16 indirectly with an external optical element. This strategy was followed by Tao *et al.* who used a  
17 ZIF-8 coated Micro Ring Resonator (MRR). Detection of Volatile Organic Compounds (VOCs)  
18 such as methanol, propylene, and benzene at concentration levels as low as ppb, was reported  
19 based on the induced refractive index (RI) changes, which detunes the MRR resonant  
20 wavelengths.<sup>35</sup> In a similar way, Kim *et al.* used a ZIF-8 coated optical fiber for monitoring a  
21 selected gas phase analyte.<sup>36</sup> Chocarro-Ruiz *et al.* recently developed an interferometric CO<sub>2</sub>  
22 sensor using a multilayer architecture which includes a Si<sub>3</sub>N<sub>4</sub> waveguide coated with an  
23 adsorbing ZIF-8 nanocrystals layer, and a final protective polydimethylsiloxane (PDMS)  
24 coating. Detection limits of such sensor are 3130 ppm at room temperature and 774 ppm at room  
25 temperature.<sup>37</sup>

1  
2  
3 MOFs' stability towards aqueous solutions, or gases/water vapor mixtures is a matter of great  
4 importance<sup>38-42</sup> in order to harness their potential in practical applications. However, the  
5 literature shows that MOFs present different degrees of stability in aqueous media<sup>43</sup> and it is  
6 actually a matter of debate. For example, XRD analysis showed that ZIF-8 colloidal dispersions  
7 remain stable at room temperature and in boiling water, even for seven days.<sup>44,45</sup> Contrary to  
8 these observations, Zhang *et al.* showed that thin  $\alpha$ -alumina supported ZIF-8 membranes are not  
9 stable towards water exposure and highly dependent on the pH value.<sup>41</sup> These examples show  
10 that characterization of both, surface and bulk properties, are necessary to address MOFs'  
11 stability in a definitive way.  
12  
13  
14  
15  
16  
17  
18  
19  
20  
21  
22

23  
24 Optical Waveguide Spectroscopy (OWS) technique and the close-related Surface Plasmon  
25 Resonance (SPR) spectroscopy, offer a convenient way for answering the above discussed  
26 questions, and eventually provide a tool for assessing changes in MOF layers exposed to  
27 different conditions. One of the earliest examples of the use of SPR and OWS for  
28 characterization of functional materials was given by Knoll.<sup>46</sup> Of course, each specific material  
29 acting as waveguide would bring new specific features for analyte detection or stimuli-  
30 responsive behavior. The review presented by Ma *et al.*<sup>47</sup> provides a compilation of a great  
31 variety of polymeric materials used as waveguides that can act as probes for many processes  
32 occurring inside nanoporous materials; e.g.,<sup>48,49</sup> characterization of block copolymers in thin  
33 films,<sup>50</sup> detection of structural changes on such films after exposure to different physical and  
34 chemical stimuli,<sup>51</sup> and variations on lateral film structure due nanoparticle incorporation.<sup>52</sup>  
35  
36  
37  
38  
39  
40  
41  
42  
43  
44  
45  
46  
47  
48

49 Synthesizing porous crystalline materials such as MOFs with the capability of acting as  
50 waveguides, opens the path not only for sensing applications but also for the observation of their  
51 structural stability. The synthesis of Lanthanide-based MOFs capable of acting as waveguides  
52  
53  
54  
55  
56  
57  
58  
59  
60

1  
2  
3 has been reported already by Yang *et al.*<sup>53</sup> Considering the physical characteristics required for a  
4 material to be used as an optical waveguide,<sup>54</sup> and the typical properties and morphologies  
5 reported for MOF films and membranes,<sup>55</sup> it might look like a difficult task to bring these two  
6 worlds together. However, Hou *et al.* showed that it is possible to achieve sufficiently uniform  
7 ZIF-8 films by a method which can be classified as Liquid-Phase Epitaxial growth, taking  
8 advantage of appropriate surface-anchoring moieties.<sup>56</sup>

9  
10 We hereby report the use of ZIF-8 MOF films as optical waveguides for the first time to the  
11 best of our knowledge. ZIF-8 optical waveguides were constructed on surface-modified gold  
12 substrates, in order to characterize film growth process and to determine structural stability  
13 towards the exposure to different aqueous environments. The suitability of this approach to  
14 elucidate the interaction of ZIF-8 films with modifying agents such as polyelectrolyte solutions  
15 (post-synthetic modification allows for the application of many different fine tuning steps in  
16 terms of material's structure-response as recently reported)<sup>19,57</sup> is demonstrated. In conjunction  
17 with effective medium theory, the optical response of ZIF-8 films can be quantified in terms of  
18 thickness, surface mass density and porosity variations, which are of the utmost importance for  
19 any sensor-related application.

## 20 21 22 23 24 25 26 27 28 29 30 31 32 33 34 35 36 37 38 39 40 41 42 **EXPERIMENTAL SECTION**

### 43 44 **Chemicals**

45 Sulfuric acid, zinc nitrate hexahydrate ( $\text{Zn}(\text{NO}_3)_2 \cdot 6\text{H}_2\text{O}$ , or ZnN), 2-methylimidazole (or  
46 HmIm), 3-mercapto-1-propanesulfonic acid sodium salt (MPSA), 70 kDa Poly(4-styrenesulfonic  
47 acid sodium salt) (NaPSS), anhydrous methanol, sodium chloride, sodium phosphate monobasic  
48 monohydrate ( $\text{NaH}_2\text{PO}_4 \cdot \text{H}_2\text{O}$ ) and sodium phosphate dibasic dihydrate ( $\text{Na}_2\text{HPO}_4 \cdot 2\text{H}_2\text{O}$ ) were  
49 purchased from Sigma Aldrich and used without further purification. Ultrapure *Milli-Q* water  
50  
51  
52  
53  
54  
55  
56  
57  
58  
59  
60

1  
2  
3 (18,24 M $\Omega$  cm) was used for all the aqueous solutions and washing steps. Further details on the  
4  
5 solutions used can be found in the supplementary information.  
6  
7  
8  
9

### 10 **Optical setup**

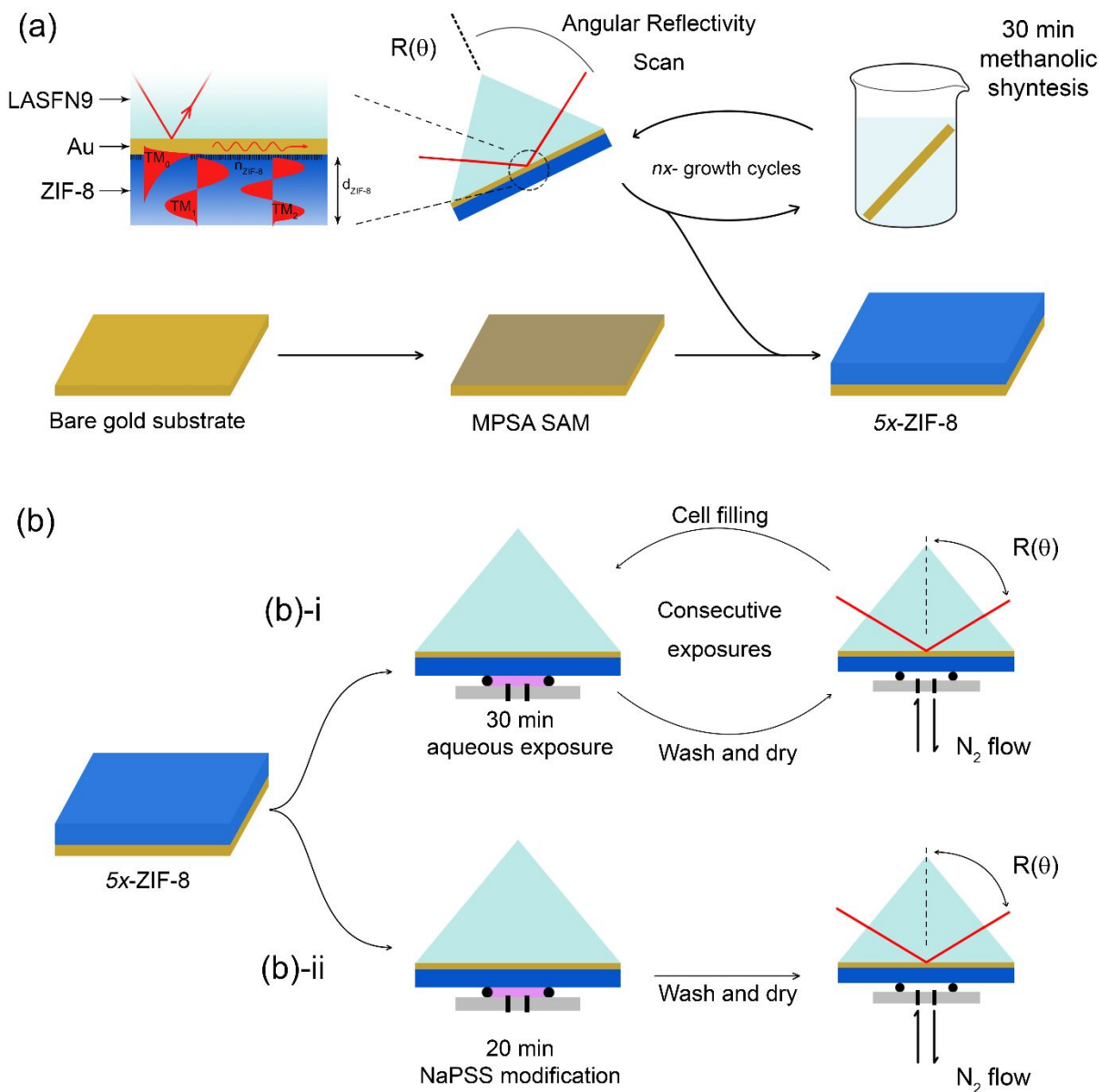
11  
12 A HeNe laser beam (2 mW,  $\lambda=632,8$  nm) was coupled to a right-angle LASFN9 glass prism in  
13  
14 an SPR spectrometer instrument, operated in the Kretschmann configuration, see scheme S1. The  
15  
16 ZIF-8 layers were grown on a LASFN9 glass substrate that was optically matched to the prism  
17  
18 base by using immersion oil. All measurements were carried out under N<sub>2</sub> flow over the ZIF-8  
19  
20 waveguide surface by using a flow-cell that was clamped at the prism base. The angle of  
21  
22 incidence  $\theta$  of the laser beam incident on the ZIF-8 surface was controlled by a rotation stage  
23  
24 (from Huber) and its polarization was set by Glan-Thompson polarizer as transverse electric  
25  
26 (TE) or transverse magnetic (TM). The intensity of laser beam reflected at prism base with ZIF-8  
27  
28 waveguide film was recorded by a photodiode detector connected to a lock-in amplifier as a  
29  
30 function of incidence angle  $R(\theta)$ . WINSPALL software (version 3.02, Max Planck Institute for  
31  
32 Polymer Research, Germany) was used to fit the experimental data  $R(\theta)$ , based on Fresnel  
33  
34 equations. In the fitting protocol, we assumed a single and isotropic layer that represents the ZIF-  
35  
36 8 waveguide layer on top of the Cr and Au layers (see supplementary information file, table S1).  
37  
38  
39  
40  
41  
42  
43  
44

### 45 **Synthesis of ZIF-8 films**

46  
47 Initially, the glass substrates were washed via subsequent 15 minutes ultrasonication steps: 1%  
48  
49 Hellmanex III solution, pure water, and ethanol. Then 50 nm thick gold layer was prepared by  
50  
51 thermal sputtering using a UNIVEX 450C apparatus (Leybold, Germany) on top of a LASFN9  
52  
53 glass substrate with a 2 nm Cr adhesion-promoting layer. ZIF-8 thin films were synthesized on  
54  
55  
56  
57  
58  
59  
60



1  
2  
3 the top of the gold surface according to previously reported protocols.<sup>19</sup> Briefly, a gold-coated  
4 substrate was placed overnight in MPSA aqueous solution. Then, the substrate was washed with  
5 *Milli-Q* pure water and dried under a stream of N<sub>2</sub>. The gold substrate with the MPSA self-  
6 assembled monolayer (SAM) exposing sulfonate-moieties was placed vertically in a 25 mM ZnN  
7 solution prepared in anhydrous methanol and then, an equal volume of 50 mM HmIm solution  
8 (also prepared in anhydrous methanol) was added. After 30 minutes, the substrate was washed  
9 generously with anhydrous methanol and dried under a N<sub>2</sub> stream. This sequence represents a  
10 single “growth cycle”. By repeating these growth cycles, it is possible to control the thickness of  
11 the formed ZIF-8 film in a step-wise manner (see Scheme 1a). The films prepared in such way  
12 will be referred to as *nx*-ZIF-8, where *n* indicates the number of growth cycles used.  
13  
14  
15  
16  
17  
18  
19  
20  
21  
22  
23  
24  
25  
26  
27  
28  
29  
30  
31  
32  
33  
34  
35  
36  
37  
38  
39  
40  
41  
42  
43  
44  
45  
46  
47  
48  
49  
50  
51  
52  
53  
54  
55  
56  
57  
58  
59  
60



**Scheme 1.** Schematics of (a) ZIF-8 film growth, (b)-i *in-situ* probing of 5x-ZIF-8 films in aqueous environments and (b)-ii *in-situ* probing of polyelectrolyte infiltration on 5x-ZIF-8 films.

### ***In-situ* probing in aqueous environment**

For *in-situ* experiments, a  $\sim 10$   $\mu\text{L}$  flow cell was mounted on top of the ZIF-8 layer surface. The cell was composed of a rubber O-ring pressed against the ZIF-8 surface by an acrylic slide

1  
2  
3 with inlet and outlet ports connected to tubing with a diameter of 0,8 mm. The flow-cell was  
4 filled with the tested solution and after the elapsed exposure time (30 minutes) in static  
5 conditions, the solution was removed from the flow-cell by using a syringe, subsequently rinsed  
6 with water, and completely dried with N<sub>2</sub> flow for 30 minutes (see scheme 1*b*-i). The N<sub>2</sub> flow  
7 was kept during the angular reflectivity scan R( $\theta$ ).  
8  
9  
10  
11  
12  
13  
14  
15  
16

### 17 ***In-situ* probing of polyelectrolyte infiltration**

18  
19 Modification with the NaPSS solution was carried *in situ*, similar to the exposure to the  
20 exposure to aqueous environments above mentioned: the polyelectrolyte solution was injected  
21 into the flow-cell for 20 minutes and then the surface was washed with water and dried in N<sub>2</sub> (see  
22 scheme 1*b*-ii). The film treated this way will be hereafter referred as *n<sub>x</sub>*-ZIF-8+PSS.  
23  
24  
25  
26  
27  
28  
29

## 30 **RESULTS AND DISCUSSION**

### 31 **Films growth and properties**

32  
33 Firstly, ZIF-8 film growth was optically characterized using resonantly excited waveguide  
34 modes. As Figure 1 shows, this excitation is manifested as a series of dips in the angular  
35 reflectivity spectrum R( $\theta$ ) in both, TM and TE polarization, which change positions after each  
36 growth cycle. The waveguide modes supported by ZIF-8 films arise from the total internal  
37 reflection of light at the outer film interface and from the reflection at the inner gold surface.  
38 Depending on the thickness  $d_{\text{ZIF-8}}$  and the refractive index  $n_{\text{ZIF-8}}$  of the film, multiple guided  
39 waves referred to as TM<sub>*m*</sub> or TE<sub>*m*</sub> (*m* is the number of nodes of that particular field distribution)  
40 can be excited with the optical beam launched into the prism and hitting the layer structure (see  
41  
42  
43  
44  
45  
46  
47  
48  
49  
50  
51  
52  
53  
54  
55  
56  
57  
58  
59  
60

1  
2  
3 Scheme 1a). The excitation of guided waves is resonant, and occurs only at specific angles ( $\theta$ ), at  
4  
5 which the laser beam is phase-matched with  $TM_m$  or  $TE_m$  modes traveling along the surface.  
6

7  
8 The synthesis of ZIF-8 film was characterized by performing angular reflectivity spectra  $R(\theta)$   
9  
10 measurements after each growth cycle. As can be seen in Figure 1,  $R(\theta)$  prior to ZIF-8 first  
11  
12 growth cycle shows one resonance in the TM polarization ( $TM_0$  mode corresponding to surface  
13  
14 plasmon – SP – at the gold/air interface) and no resonance in TE polarization. After the first  
15  
16 cycle of ZIF-8 growth, the resonant angle at which the SP is excited shifts by almost  $30^\circ$  and the  
17  
18 excitation of the first guided mode  $TE_0$  occurs in TE polarization. With the subsequent growth  
19  
20 cycles ( $nx = 2x, 3x...5x$ ), the SP angular position does not change significantly,  $TE_0$  guided mode  
21  
22 shifts to higher angular values, and additional higher order guided modes in both TM and TE  
23  
24 polarizations, respectively, occur. After the complete film synthesis (five growth cycles),  $TM_0$   
25  
26 (SP) and four guided modes  $TE_{0,1}$  and  $TM_{1,2}$  are observed. The measured reflectivity curves  $R(\theta)$   
27  
28 have been fitted with a Fresnel reflectivity-based model in order to determine changes in the  
29  
30 thickness  $d_{ZIF-8}$  and refractive index  $n_{ZIF-8}$  of the synthesized ZIF-8 films. For the first growth  
31  
32 cycle, the fitting of two observed resonances due to SP and  $TE_0$  mode, allows for determination  
33  
34 of both  $d_{ZIF-8}=174\pm 4$  nm, and  $n_{ZIF-8}=1,357\pm 0,005$  parameters. For the films obtained after  
35  
36 subsequent growth cycles ( $nx = 2x$  to  $5x$ ), fitting all the observed resonances becomes not  
37  
38 possible using the model, and the experimental SP angular position exhibits a slight deviation  
39  
40 (between  $1^\circ$  and  $1,3^\circ$ ) respecting to the fit. This difference can be attributed to the fact that  
41  
42 probing distance of the SP is only around 100 nm from the gold surface, and thus it only partially  
43  
44 overlaps with the first layer and it does not allow for probing of the increased thickness gained  
45  
46 after additional synthesis steps. On the contrary, the guided modes  $TM_{1,2}$  and  $TE_{0,1}$  exhibit a  
47  
48 more delocalized profile of electromagnetic field, and thus probe the entire thickness of ZIF-8  
49  
50  
51  
52  
53  
54  
55  
56  
57  
58  
59  
60

layer. These discrepancies indicate that effective optical properties of ZIF-8 films at the very interface with the gold surface (as observed via SP mode variations) may be slightly different than those values obtained from thickness-averaged determinations when probing the entire structure (as observed by  $TM_{1,2}$  and  $TE_{0,1}$ ). Further discussion addressing this point will be given, together with MPSA monolayer effect (see below).

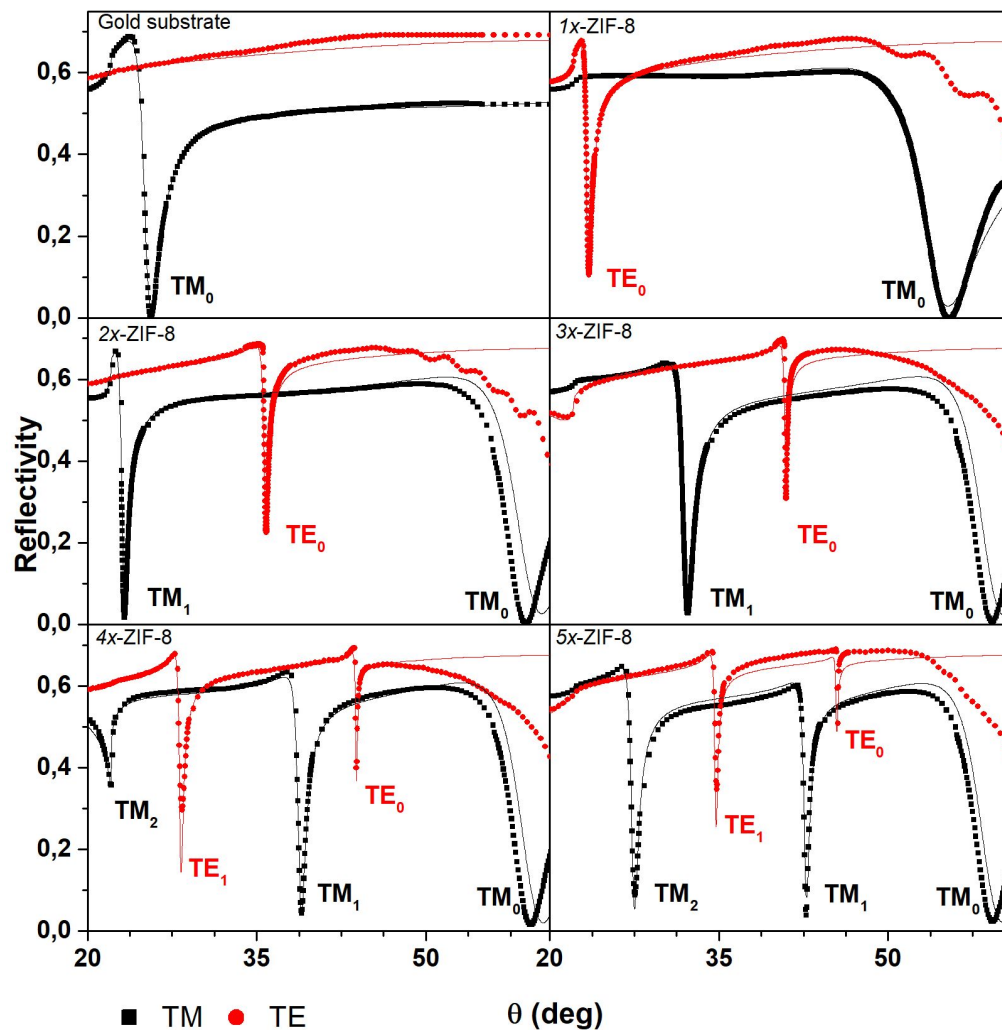
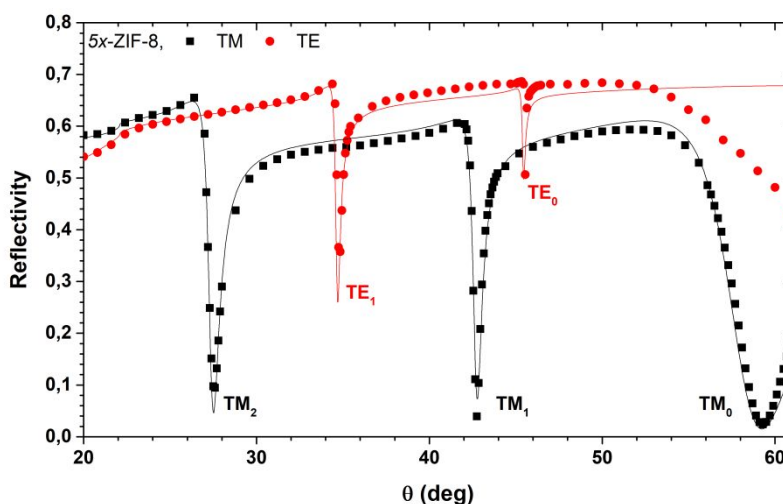


**Figure 1.** Cycle-by-cycle progression of the resonant coupling of guided modes under TM (black squares) and TE (red circles) polarization, and model fitting (full lines) for the 5x-ZIF-8 film construction.

1  
2  
3 It is possible to tackle the problem of the observed difference between the experimental and  
4 fitted curves for the SP angular position by adopting a slightly more complex bilayer model.  
5 Under this approach, the first layer would have the thickness found for the  $1x$ -ZIF-8 films, while  
6 the thickness of the second layer will change according to the increasing number of growth  
7 cycles (total thickness would be the sum of both assumed layers). Regarding the refractive index  
8 (RI), the values would change for each layer, in order to correctly fit the experimental curves.  
9  
10 Fig. 2 shows as an example of how the two-layer model describes accurately the SP resonant  
11 angular position as well as all the guided modes.  
12  
13  
14  
15  
16  
17  
18  
19  
20  
21



22  
23  
24  
25  
26  
27  
28  
29  
30  
31  
32  
33  
34  
35  
36  
37  
38 **Figure. 2:** Resonant coupling for the 5x-ZIF-8 film under TM (black squares) and TE (red  
39 circles) polarization. Experimental points were fitted with a bilayer model (full line).  
40  
41  
42  
43

44 Although there is better agreement between experiments and fittings when using this two-  
45 layer model, the parameters obtained are quite similar to what is obtained using the much simpler  
46 one-layer model; *e.g.*, thickness progression was found to be exactly the same ( $138 \pm 3$  nm/cycle).  
47 However, the two-layer model results in a RI value for the first layer which is lower than the RI  
48 obtained for the second layer. Moreover, having in mind that film porosity should only depend  
49 on its crystalline structure, one can safely disregard the two-layer model, since the porous  
50  
51  
52  
53  
54  
55  
56  
57  
58  
59  
60

1  
2  
3 fraction was found to be larger for the first layer than for the second layer after applying  
4 Bruggeman's theory. Additionally, structural stability of ZIF-8 film after post-synthetic  
5 modifications (see below) can be better understood by assuming the existence of a single unit  
6 rather than a two-layer structure. Based on the above discussion, we selected the one-layer model  
7 for describing the observed behavior.  
8  
9

10  
11  
12 The parameters  $d_{\text{ZIF-8}}$  and  $n_{\text{ZIF-8}}$  were determined for each subsequent growth cycle, as  
13 presented in the supplementary information (Table S2). Evolution of film thickness is shown in  
14 Figure 3. These experiments reveal a linear increase in the thickness per growth cycle with a  
15 slope of  $138 \pm 3$  nm/cycle. The standard deviation in thickness of about 2% indicates a highly  
16 reproducible synthesis process as determined by comparing four equivalent 5x-ZIF-8 films, each  
17 of which was measured and fitted on three different spots. From this analysis, it was also  
18 possible to calculate an average real part of the refractive index of ZIF-8:  $\text{Re}\{n_{\text{ZIF-8}}\} = 1,352 \pm 0,004$   
19 at  $\lambda = 632,8$  nm, in good agreement with previously reported values.<sup>42</sup> Using the  
20 Bruggeman's Effective Medium Theory (calculation details can be found in the supporting  
21 information) porous fraction of 0,6 was determined for all prepared 5x-ZIF-8 films. This result is  
22 in line with previously reported porosity values for similar ZIF-8 crystals (58,8 %).<sup>58</sup>  
23  
24  
25  
26  
27  
28  
29  
30  
31  
32  
33  
34  
35  
36  
37  
38  
39  
40  
41  
42  
43  
44  
45  
46  
47  
48  
49  
50  
51  
52  
53  
54  
55  
56  
57  
58  
59  
60

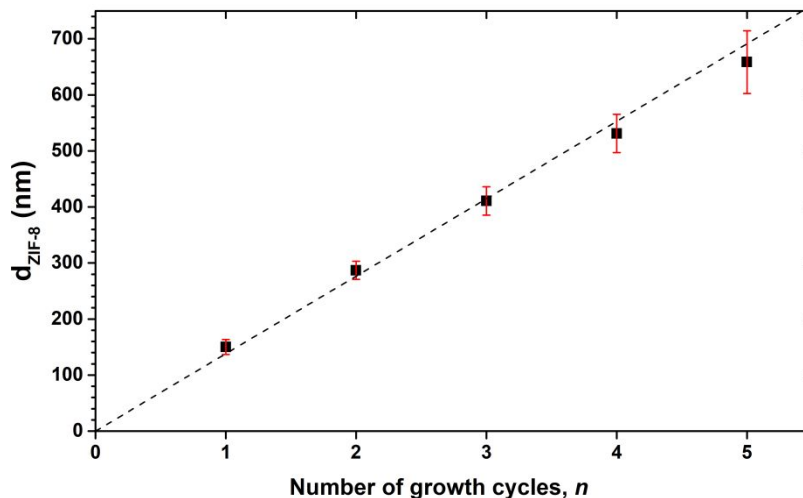


**Figure 3.** Thickness evolution ( $d_{\text{ZIF-8}}$ ) upon sequential synthesis of 5x-ZIF-8 films. Each value was averaged from measurements on 4 different samples and 3 distinct spots. Error bars correspond to standard errors and the dashed line represents the linear fit ( $r^2 = 0,998$ ) of the measured values.

Interestingly, the observed growth rate of  $138 \pm 3$  nm/cycle is significantly higher than what previously reported in the literature ( $\sim 70$  nm/cycle)<sup>56</sup>. This difference can be ascribed to the effect of sulfonate moieties introduced to the gold interface by the MPSA SAM primer.<sup>59,60</sup> These anchoring moieties are crucial for obtaining an homogenous ZIF-8 layer that can serve as an efficient slab waveguide. For comparison, Figure S1 (see supporting information) shows the progression of the angular reflectivity scans  $R(\theta)$  for the growth of ZIF-8 at bare gold surfaces; *i.e.*, without MPSA. The experiment reveals that the angular width of  $\text{TM}_0$  (SP) resonance is significantly broader and that higher waveguide modes are not apparent. This can be ascribed to the strongly deteriorated lateral homogeneity of the ZIF-8 film, which can be quantified by the use of the effective extinction coefficient  $\kappa$  of the ZIF-8 layer (imaginary part of the refractive index  $\text{Im}\{n_{\text{ZIF-8}}\}$ ). This parameter can be determined by the fitting analysis of  $R(\theta)$  and



1  
2  
3 increasing  $\kappa$  is typically associated with a broadening of the observed dips in  $R(\theta)$ . Effective  
4 extinction coefficient  $\kappa$  takes into account scattering on defects with a size comparable or higher  
5 than the used wavelength  $\lambda$  and it is important to note neither  $Zn^{2+}$  nor  $mIm^-$  (which are used to  
6 synthesize the ZIF-8 films) exhibit absorption at selected wavelength  $\lambda$ .  
7  
8  
9  
10

11 Table 1 provides the comparison of thickness  $d_{ZIF-8}$  and extinction coefficient  $\kappa$  determined for  
12 the films prepared on a gold surface without and with an MPSA SAM. MPSA was expected to  
13 promote heterogeneous nucleation of ZIF-8 on the surface triggered by pre-coordination of  $Zn^{2+}$   
14 ions by the surface-exposed sulfonate moieties.<sup>60</sup> There were two main results supporting the  
15 assumption above. First, thickness value  $d_{ZIF-8}$  for the  $1x$ -ZIF-8 is almost 20 times higher when  
16 using MPSA anchoring, but for the next growth cycles these differences start to decrease, and at  
17 the end,  $5x$ -ZIF-8 synthesized on an MPSA SAM is only 1,5 times greater than when no MPSA  
18 SAM is present. Second, the extinction coefficient  $\kappa$  of films prepared on MPSA SAM is at least  
19 one order of magnitude lower than that without this anchoring layer. In other words, by  
20 providing these initial nucleation points distributed across the gold surface, a higher density of  
21 (probably smaller) nuclei is achieved, and ultimately causes a much more homogeneous film  
22 compared to what is obtained when nucleation occurs preferentially in the homogeneous phase  
23 and nanocrystals thus formed start to aggregate to form the film. The fact that the extinction  
24 coefficient  $\kappa$  decreases with film growth progression over MPSA SAM also supports the  
25 hypothesis, as each growth cycle is influenced by the presence of the previously synthesized  
26 ZIF-8 layer. The above interpretation brings further support for the use of a single layer model to  
27 describe the system; *i.e.*, each growth cycle does not generate layers with different morphology  
28 but rather contribute to a one-block structure with increasing thickness.  
29  
30  
31  
32  
33  
34  
35  
36  
37  
38  
39  
40  
41  
42  
43  
44  
45  
46  
47  
48  
49  
50  
51  
52  
53  
54  
55  
56  
57  
58  
59  
60

Growth Cycle ( $nx$ )	Thickness $d_{\text{ZIF-8}}$ (nm)		ratio	Ext. coefficient $\kappa$		ratio
	With MPSA	Without MPSA	$d_{\text{wo}}/d_{\text{w}}$	With MPSA	Without MPSA	$\kappa_{\text{wo}}/\kappa_{\text{w}}$
1	150	8,8	0,06	0,0035	0,312	89
2	287	39	0,14	0,0030	0,276	92
3	410	91	0,22	0,0016	0,150	94
4	530	359	0,68	0,0017	0,049	29
5	658	426	0,65	0,0017	0,036	21

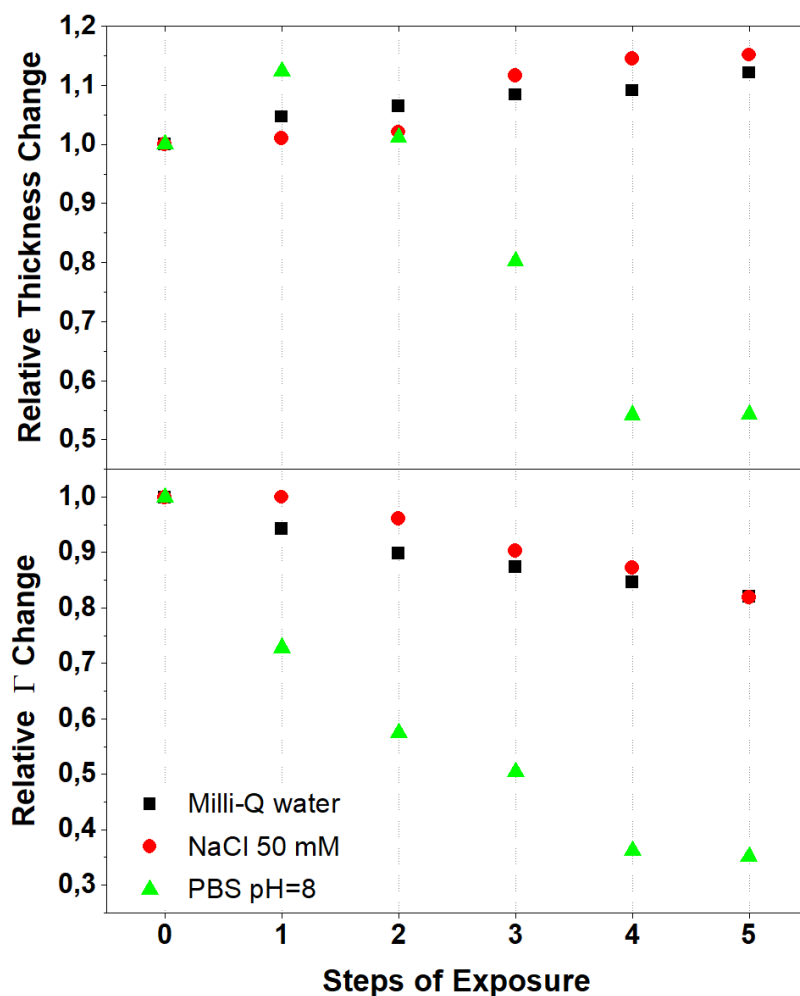
**Table 1.** Comparison of thickness ( $d_{\text{ZIF-8}}$ ) and extinction coefficient ( $\kappa$ ) for 5x-ZIF-8 films synthesized on a gold surface with and without an MPSA nucleation layer.

### Structural stability of ZIF-8 films in aqueous environment

The stability of the ZIF-8 film is crucial for determining its possible applications. A useful quantity to evaluate this feature is the layer surface mass density  $\Gamma$ , which takes into account the potential loss in the porous material due to etching caused by exposure to different solvents. Surface mass density can be shown to be proportional to the term  $d_{\text{ZIF-8}}(1-f_{\text{pores}})$ , where the volume fraction of pores  $f_{\text{pores}}$  can be obtained from fitted  $\text{Re}\{n_{\text{ZIF-8}}\}$  by Bruggeman effective medium theory (see supporting information).

In order to study the stability of synthesized materials, 5x-ZIF-8 films were investigated after they were exposed to *Milli-Q* water, NaCl 50 mM aqueous solution, and finally to 10 mM PBS, pH=8, aqueous buffer. NaCl was chosen in order to regulate ionic strength because  $\text{Na}^+$  and  $\text{Cl}^-$  ions were proved to have no effect on the crystalline structure of ZIF-8.<sup>61,62</sup> Figure 4 shows the relative changes between final and initial thicknesses as  $(d_{\text{ZIF-8}}^f - d_{\text{ZIF-8}}^i)/d_{\text{ZIF-8}}^i$  (top), and the relative changes between final and initial  $\Gamma$  as  $(\Gamma_f - \Gamma_i)/\Gamma_i$  (bottom) after sequential (30 min)

static exposure to each of the above solutions. Results obtained reveal that films exposed to Milli-Q water and NaCl experiment some swelling; a 15% thickness increase was detected compared to what observed for freshly prepared films after five exposure cycles (equivalent to 150 min). Such swelling is accompanied with a decrease in surface mass density  $\Gamma$ , which reaches a 20% loss of ZIF-8 mass after five exposures (see table S3 for the further details). Interestingly, ZIF-8 films were found to behave dramatically different in PBS solution. The film underwent an initial thickness increase by 12% after 30 min exposure of PBS followed by a gradual decrease to a final value of 50% after five exposure cycles. In addition,  $\Gamma$  shows a continuous decrease until a loss of almost 65%.



1  
2  
3 **Figure 4.** Relative changes on Thickness (top) and  $\Gamma$  (bottom) for 5x-ZIF-8 films after five  
4 consecutive 30 min exposures to *Milli-Q* water (black squares), 50 mM NaCl (red circles) and 10  
5 mM PBS, pH=8 (green triangles).  
6  
7  
8  
9

10  
11  
12 The observed changes in  $\Gamma$  can be ascribed to variations in the thickness as well as in the  
13 porous fraction,  $f_{\text{pores}}$ . Figure 5 provides this information, which confirms that ZIF-8 films  
14 gradually undergo an irreversible swelling together with a release of occluded material when  
15 exposed to *Milli-Q* and NaCl 50 mM solution. Contrary to these experiments, the porous fraction  
16  $f_{\text{pores}}$  abruptly increases by 20% after the first exposure to PBS and afterward it does not change  
17 substantially. These observations indicate that, after exposure to *Milli-Q* water and 50 mM NaCl  
18 solution, the film slowly swells and the porosity  $f_{\text{pores}}$  increases. On the other hand, exposure to  
19 PBS causes the film to experience an initial thickness increase followed by a gradual material  
20 loss without collapsing, which decreases its thickness although porosity shows no variation. It is  
21 worth mentioning that Wang et al. already reported such effect for ZIF-8 exposed to PBS  
22 solutions<sup>61</sup> but higher pH values were used (9,0 and 13,2), for which the material is not expected  
23 to be stable towards hydrolysis. Additionally, in the same reported work, higher concentrations  
24 were used which translates to almost 100 mM ionic strength and means that no direct  
25 comparison is possible to the results hereby presented.  
26  
27  
28  
29  
30  
31  
32  
33  
34  
35  
36  
37  
38  
39  
40  
41  
42  
43  
44  
45  
46  
47  
48  
49  
50  
51  
52  
53  
54  
55  
56  
57  
58  
59  
60

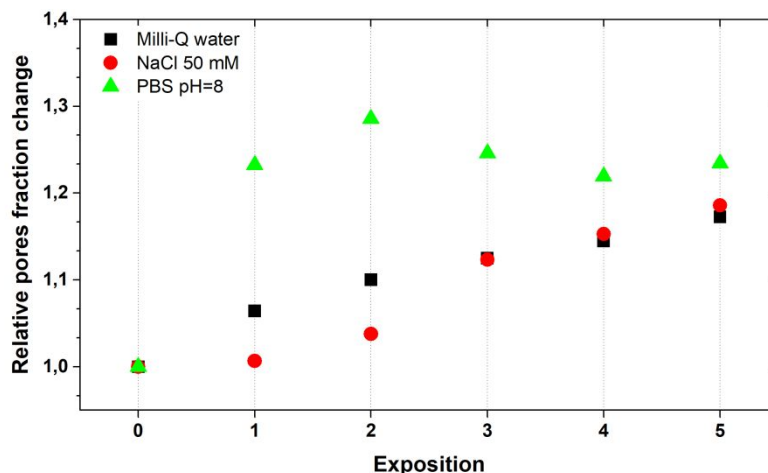


**Figure 5.** Relative porous fraction change for 5x-ZIF-8 films after five consecutive exposures to Milli-Q water (black squares), 50 mM NaCl (red circles) and 10 mM PBS, pH=8 (green triangles).

### Polyelectrolyte/ZIF-8 interaction

It was previously reported that PSS can modify the polar character of ZIF-8 films' porosity, which in turn, alters effective diffusion coefficients.<sup>19</sup> This opens the path for the use of diffusion-reaction approach for the synthesis of film-embedded metal nanoparticles. The successful polyelectrolyte capping of films constituted by porous materials depends on the nature and strength of the interactions between capping agent and the pore walls. Possible architectures obtained are either confined (polyelectrolyte remains segregated on a different phase causing no effect on the porous material) or segregated (polyelectrolyte percolates the entire porous structure causing a change on the overall films' polar character). In order to gain insight into the outcome of such processes, a series of OWS measurements were carried out on films that were

1  
2  
3 exposed to PSS polymer solutions (PSS was selected due to both its anionic nature and its  
4 affinity towards  $Zn^{2+}$  moieties on ZIF-8). Figure 6 shows a comparison of reflectivity curves  
5  $R(\theta)$  before (5x-ZIF-8) and after modification with PSS (5x-ZIF-8+PSS). These curves reveal  
6 that the angles at which the resonant coupling to guided waves occurs are shifted by about  $3^\circ$ . By  
7 fitting experimental data obtained, a (relatively) strong increase in RI from  $n_{ZIF-8}=1,352$  to 1,375  
8 was determined, together with a small (1,74%) increase of film thickness  $d_{ZIF-8}$ . Since the strong  
9 refractive index increase relates to a decrease in  $f_{pores}$ , it can be assumed that PSS efficiently  
10 percolates the entire film. This assumption is supported by the fact that, if the PSS would remain  
11 mostly surface-confined, the SP ( $TM_0$ ) resonance angular position should not change. However,  
12 the surface plasmon waves probing the gold/ZIF-8 interface, show a distinct angular change  
13 which indicates that PSS was distributed through the whole film (see supporting information).  
14 Although the experimental data was successfully fitted by using a single and isotropic layer, the  
15 observed shifts on the different guided modes allow for hypothesizing that, even though PSS  
16 percolates the whole film structure, some lateral gradient concentration of PSS could be  
17 expected. By applying effective medium theory, it was possible to calculate the remaining  
18 porous fraction after PSS modification and to obtain an estimation of the polymer fraction in the  
19 film (see supporting information). Briefly, the final composition obtained was 40,9% of ZIF-8  
20 (framework), 55,2% empty pores, and 3,9% of polymer. It is possible to say thus, that PSS  
21 modification does not represent a significant decrease in film porosity, which is a core property  
22 when thinking MOFs as sensing platforms.  
23  
24  
25  
26  
27  
28  
29  
30  
31  
32  
33  
34  
35  
36  
37  
38  
39  
40  
41  
42  
43  
44  
45  
46  
47  
48  
49  
50  
51  
52  
53  
54  
55  
56  
57  
58  
59  
60

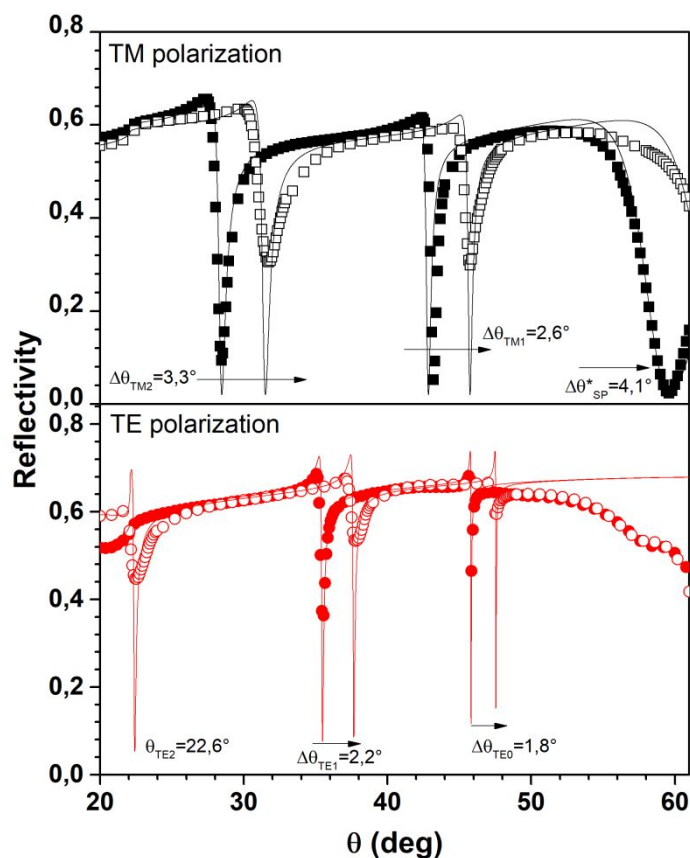


**Figure 6.** Resonant coupling of guided modes under TM (black squares, top) and TE (red circles, bottom) polarization for a 5x-ZIF-8 film (filled dots) and 5x-ZIF-8+PSS film (empty dots).

## CONCLUSIONS

Surface plasmon resonance in combination with optical waveguide spectroscopy provided new insight into the growth and structural stability of ZIF-8 films towards exposure to aqueous solutions relevant for a wide range of applications. For this end, we have for the first-time synthesized wave-guiding MOF-films. We have found a linear thickness increase for films growth cycles and showed how each of those cycles is strongly influenced by the previous step in terms of the chemical identity of the starting layer. The experimental setup used allowed us to

1  
2  
3 confirm that substrate surface modification with MPSA monolayer primer is critical in order to  
4  
5 achieve ZIF-8 layers that can effectively act as monomode or multimode slab optical  
6  
7 waveguides. We have shown also, that ZIF-8 films are structurally stable under *Milli-Q* water  
8  
9 and NaCl 50 mM solutions, and that the choice of a proper buffered media needs to be carefully  
10  
11 considered (i.e., PBS buffer was shown to be deleterious for film stability in the case of ZIF-8  
12  
13 MOF). It was demonstrated that polyelectrolyte post-synthetic modification of ZIF-8 films  
14  
15 modify their surface properties without detrimental effects on the porosity, thus providing a  
16  
17 powerful tool for fine-tuning their transport properties.  
18  
19  
20  
21  
22  
23

## 24 **Supporting Information**

25  
26 The Supporting Information is available free of charge on the ACS website: A brief description of OWS-  
27  
28 SPR technique as well as experimental relevant data.  
29  
30  
31  
32  
33  
34

## 35 **Acknowledgments**

36  
37  
38  
39  
40 This work was supported by the European Union's Horizon 2020 under the Marie Curie grant  
41  
42 agreement No. 645686, CONICET, ANPCyT (PICT-2010-2554, PICT 2013-0905), the Austrian  
43  
44 Institute of Technology GmbH (AIT-CONICET Partner Group, Exp. 4947/11, Res. No. 3911,  
45  
46 28-12-2011), Universidad Nacional de La Plata (UNLP), the Austrian Federal ministry for  
47  
48 Transportation, Innovation and Technology (GZ BMVIT-612.166/0001-III/I1/2010), by the FFG  
49  
50 within the comet program, and from the governments of Lower and Upper Austria. J.A.A. wants  
51  
52  
53  
54  
55  
56  
57  
58  
59  
60



1  
2  
3 to acknowledge CONICET for his doctoral scholarship and the Biosensor Technologies group  
4  
5 for the support and help during his stay at AIT.  
6  
7  
8  
9  
10  
11  
12  
13  
14  
15  
16  
17  
18  
19  
20  
21  
22  
23  
24  
25  
26  
27  
28  
29  
30  
31  
32  
33  
34  
35  
36  
37  
38  
39  
40  
41  
42  
43  
44  
45  
46  
47  
48  
49  
50  
51  
52  
53  
54  
55  
56  
57  
58  
59  
60

## REFERENCES

- (1) Férey, G. Hybrid Porous Solids: Past, Present, Future. *Chem. Soc. Rev.* **2008**, *37* (1), 191–214.
- (2) Furukawa, H.; Cordova, K. E.; O’Keeffe, M.; Yaghi, O. M. The Chemistry and Applications of Metal–Organic Frameworks. *Science* **2013**, *341* (6149), 1230444.
- (3) Xiang, S.; Zhou, W.; Gallegos, J. M.; Liu, Y.; Chen, B. Exceptionally High Acetylene Uptake in a Microporous Metal–Organic Framework with Open Metal Sites. *J. Am. Chem. Soc.* **2009**, *131* (34), 12415–12419.
- (4) Li, J.-R.; Sculley, J.; Zhou, H.-C. Metal–Organic Frameworks for Separations. *Chem. Rev.* **2012**, *112* (2), 869–932.
- (5) Della Rocca, J.; Liu, D.; Lin, W. Nanoscale Metal–Organic Frameworks for Biomedical Imaging and Drug Delivery. *Acc. Chem. Res.* **2011**, *44* (10), 957–968.
- (6) Li, J.-R.; Ma, Y.; McCarthy, M. C.; Sculley, J.; Yu, J.; Jeong, H.-K.; Balbuena, P. B.; Zhou, H.-C. Carbon Dioxide Capture-Related Gas Adsorption and Separation in Metal–Organic Frameworks. *Coord. Chem. Rev.* **2011**, *255* (15–16), 1791–1823.
- (7) Park, J.; Wang, Z. U.; Sun, L.-B.; Chen, Y.-P.; Zhou, H.-C. Introduction of Functionalized Mesopores to Metal–Organic Frameworks via Metal–Ligand–Fragment Coassembly. *J. Am. Chem. Soc.* **2012**, *134* (49), 20110–20116.
- (8) Cohen, S. M. Postsynthetic Methods for the Functionalization of Metal–Organic Frameworks. *Chem. Rev.* **2012**, *112* (2), 970–1000.
- (9) Gascon, J.; Corma, A.; Kapteijn, F.; Llabrés i Xamena, F. X. Metal Organic Framework Catalysis: Quo Vadis ? *ACS Catal.* **2014**, *4* (2), 361–378.
- (10) Fracaroli, A. M.; Siman, P.; Nagib, D. A.; Suzuki, M.; Furukawa, H.; Toste, F. D.; Yaghi, O. M. Seven Post-Synthetic Covalent Reactions in Tandem Leading to Enzyme-like Complexity within Metal–Organic Framework Crystals. *J. Am. Chem. Soc.* **2016**, *138* (27), 8352–8355.
- (11) Wang, C.; Tuninetti, J.; WANG, Z.; Zhang, C.; Ciganda, R.; Salmon, L.; Moya, S.; Ruiz, J.; Astruc, D. Hydrolysis of Ammonia-Borane over Ni/ZIF-8 Nanocatalyst: High Efficiency, Mechanism and Controlled Hydrogen Release. *J. Am. Chem. Soc.* **2017**, *139*(33), 11610–11615.
- (12) Shekhah, O. Layer-by-Layer Method for the Synthesis and Growth of Surface Mounted Metal–Organic Frameworks (SURMOFs). *Materials*. **2010**, *3* (2), 1302–1315.
- (13) Liu, B.; Ma, M.; Zacher, D.; Bétard, A.; Yusenko, K.; Metzler-Nolte, N.; Wöll, C.; Fischer, R. a. Chemistry of SURMOFs: Layer-Selective Installation of Functional Groups and Post-Synthetic Covalent Modification Probed by Fluorescence Microscopy. *J. Am. Chem. Soc.* **2011**, *133* (6), 1734–1737.

- 1  
2  
3 (14) Arslan, H. K.; Shekhah, O.; Wohlgemuth, J.; Franzreb, M.; Fischer, R. A.; Wöll, C. High-  
4 Throughput Fabrication of Uniform and Homogenous MOF Coatings. *Adv. Funct. Mater.*  
5 **2011**, *21* (22), 4228–4231.  
6  
7 (15) Brunsen, A.; Cui, J.; Ceolín, M.; Campo, A. del; Soler-Illia, G. J. A. A.; Azzaroni, O.  
8 Light-Activated Gating and Permselectivity in Interfacial Architectures Combining  
9 “Caged” Polymer Brushes and Mesoporous Thin Films. *Chem. Commun.* **2012**, *48* (10),  
10 1422–1424.  
11  
12 (16) Andrieu-Brunsen, A.; Micoureau, S.; Tagliacucchi, M.; Szleifer, I.; Azzaroni, O.; Soler-  
13 Illia, G. J. A. A. Mesoporous Hybrid Thin Film Membranes with PMETAC@Silica  
14 Architectures: Controlling Ionic Gating through the Tuning of Polyelectrolyte Density.  
15 *Chem. Mater.* **2015**, *27* (3), 808–821.  
16  
17 (17) Fu, Q.; Rao, G. V. R.; Ista, L. K.; Wu, Y.; Andrzejewski, B. P.; Sklar, L. A.; Ward, T. L.;  
18 López, G. P. Control of Molecular Transport Through Stimuli-Responsive Ordered  
19 Mesoporous Materials. *Adv. Mater.* **2003**, *15* (15), 1262–1266.  
20  
21 (18) Calvo, A.; Yameen, B.; Williams, F. J.; Azzaroni, O.; Soler-Illia, G. J. A. A. Facile  
22 Molecular Design of Hybrid Functional Assemblies with Controllable Transport  
23 Properties: Mesoporous Films Meet Polyelectrolyte Brushes. *Chem. Commun.* **2009**, *18*,  
24 2553–2555.  
25  
26 (19) Allegretto, J. A.; Tuninetti, J. S.; Lorenzo, A.; Ceolín, M.; Azzaroni, O.; Rafti, M.  
27 Polyelectrolyte Capping As Straightforward Approach toward Manipulation of Diffusive  
28 Transport in MOF Films. *Langmuir* **2018**, *34* (1), 425–431.  
29  
30 (20) Zhang, K.; Lively, R. P.; Zhang, C.; Koros, W. J.; Chance, R. R. Investigating the Intrinsic  
31 Ethanol/Water Separation Capability of ZIF-8: An Adsorption and Diffusion Study. *J.*  
32 *Phys. Chem. C* **2013**, *117* (14), 7214–7225.  
33  
34 (21) Gee, J. A.; Chung, J.; Nair, S.; Sholl, D. S. Adsorption and Diffusion of Small Alcohols in  
35 Zeolitic Imidazolate Frameworks ZIF-8 and ZIF-90. *J. Phys. Chem. C* **2013**, *117* (6),  
36 3169–3176.  
37  
38 (22) Wang, B.; Côté, A. P.; Furukawa, H.; O’Keeffe, M.; Yaghi, O. M.; O’Keeffe, M.; Yaghi,  
39 O. M. Colossal Cages in Zeolitic Imidazolate Frameworks as Selective Carbon Dioxide  
40 Reservoirs. *Nature* **2008**, *453* (7192), 207–211.  
41  
42 (23) Barankova, E.; Tan, X.; Villalobos, L. F.; Litwiller, E.; Peinemann, K.-V. A Metal  
43 Chelating Porous Polymeric Support: The Missing Link for a Defect-Free Metal-Organic  
44 Framework Composite Membrane. *Angew. Chemie Int. Ed.* **2017**, 1–5.  
45  
46 (24) Pan, Y.; Liu, W.; Zhao, Y.; Wang, C.; Lai, Z. Improved ZIF-8 Membrane: Effect of  
47 Activation Procedure and Determination of Diffusivities of Light Hydrocarbons. *J. Memb.*  
48 *Sci.* **2015**, *493*, 88–96.  
49  
50 (25) Jomekian, A.; Behbahani, R. M.; Mohammadi, T.; Kargari, A. Innovative Layer by Layer  
51 and Continuous Growth Methods for Synthesis of ZIF-8 Membrane on Porous Polymeric  
52  
53  
54  
55  
56  
57  
58  
59  
60

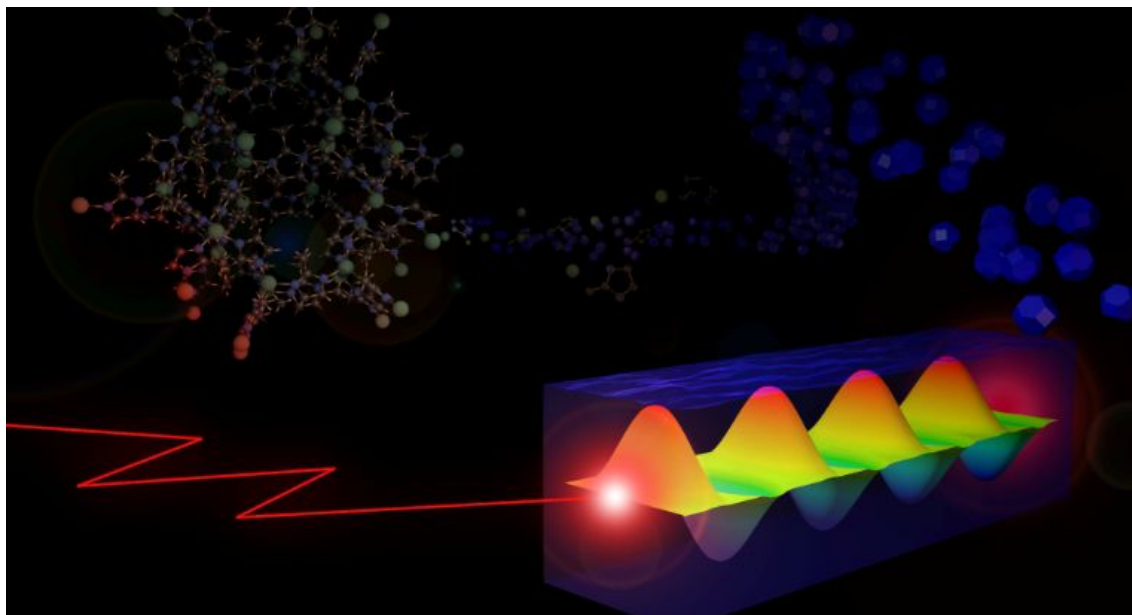
- Support Using Poly(Ether-Block-Amide) as Structure Directing Agent for Gas Separation. *Microporous Mesoporous Mater.* **2016**, *234*, 43–54.
- (26) Liu, Y.; Li, S.; Zhang, X.; Liu, H.; Qiu, J.; Li, Y.; Yeung, K. L. New Membrane Architecture: ZnO@ZIF-8 Mixed Matrix Membrane Exhibiting Superb H<sub>2</sub> Permselectivity and Excellent Stability. *Inorg. Chem. Commun.* **2014**, *48*, 77–80.
- (27) Yang, L.; Wang, Z.; Zhang, J. Zeolite Imidazolate Framework Hybrid Nanofiltration (NF) Membranes with Enhanced Permselectivity for Dye Removal. *J. Memb. Sci.* **2017**, *532*, 76–86.
- (28) Marti, A. M.; Wickramanayake, W.; Dahe, G.; Sekizkardes, A.; Bank, T. L.; Hopkinson, D. P.; Venna, S. R. Continuous Flow Processing of ZIF-8 Membranes on Polymeric Porous Hollow Fiber Supports for CO<sub>2</sub> Capture. *ACS Appl. Mater. Interfaces* **2017**, *9*(7), 5678-5682.
- (29) Hess, S. C.; Grass, R. N.; Stark, W. J. MOF Channels within Porous Polymer Film: Flexible, Self-Supporting ZIF-8 Polyethersulfone Composite Membrane. *Chem. Mater.* **2016**, *28*(21), 7638-7644.
- (30) Demessence, A.; Boissière, C.; Grosso, D.; Horcajada, P.; Serre, C.; Férey, G.; Soler-Illia, G. J. A. A.; Sanchez, C. Adsorption Properties in High Optical Quality NanoZIF-8 Thin Films with Tunable Thickness. *J. Mater. Chem.* **2010**, *20* (36), 7676.
- (31) Eslava, S.; Zhang, L.; Esconjauregui, S.; Yang, J.; Vanstreels, K.; Baklanov, M. R.; Saiz, E. Metal-Organic Framework ZIF-8 Films As Low- $\kappa$  Dielectrics in Microelectronics. *Chem. Mater.* **2013**, *25* (1), 27–33.
- (32) Li, W. J.; Gao, S. Y.; Liu, T. F.; Han, L. W.; Lin, Z. J.; Cao, R. In Situ Growth of Metal-Organic Framework Thin Films with Gas Sensing and Molecule Storage Properties. *Langmuir* **2013**, *29* (27), 8657–8664.
- (33) Lu, G.; Hupp, J. T. Metal–Organic Frameworks as Sensors: A ZIF-8 Based Fabry–Pérot Device as a Selective Sensor for Chemical Vapors and Gases. *J. Am. Chem. Soc.* **2010**, *132* (23), 7832–7833.
- (34) Li, L.; Jiao, X.; Chen, D.; Lotsch, B. V.; Li, C. Facile Fabrication of Ultrathin Metal-Organic Framework-Coated Monolayer Colloidal Crystals for Highly Efficient Vapor Sensing. *Chem. Mater.* **2015**, *27* (22), 7601–7609.
- (35) Tao, J.; Wang, X.; Sun, T.; Cai, H.; Wang, Y.; Lin, T.; Fu, D.; Ting, L. L. Y.; Gu, Y.; Zhao, D. Hybrid Photonic Cavity with Metal-Organic Framework Coatings for the Ultra-Sensitive Detection of Volatile Organic Compounds with High Immunity to Humidity. *Sci. Rep.* **2017**, *7*, 41640.
- (36) Kim, K.-J.; Lu, P.; Culp, J. T.; Ohodnicki, P. R. Metal-Organic Framework Thin Film Coated Optical Fiber Sensors: A Novel Waveguide-Based Chemical Sensing Platform. *ACS Sensors* **2018**, *3*(2), 386-394.
- (37) Chocarro-Ruiz, B.; Pérez-Carvajal, J.; Avci, C.; Calvo-Lozano, O.; Alonso, M. I.;

- Maspoch, D.; Lechuga, L. M. A CO<sub>2</sub> Optical Sensor Based on Self-Assembled Metal–organic Framework Nanoparticles. *J. Mater. Chem. A* **2018**, *6* (27), 13171–13177.
- (38) Pang, S. H.; Han, C.; Sholl, D. S.; Jones, C. W.; Lively, R. P. Facet-Specific Stability of ZIF-8 in the Presence of Acid Gases Dissolved in Aqueous Solutions. *Chem. Mater.* **2016**, *28*(19), 6960–6967.
- (39) Bhattacharyya, S.; Han, R.; Kim, W.-G.; Chiang, Y.; Jayachandrababu, K. C.; Hungerford, J. T.; Dutzer, M. R.; Ma, C.; Walton, K. S.; Sholl, D. S.; Nair, S. Acid Gas Stability of Zeolitic Imidazolate Frameworks: Generalized Kinetic and Thermodynamic Characteristics. *Chem. Mater.* **2018**, *30* (12), 4089–4101.
- (40) Dutta, A.; Tymińska, N.; Zhu, G.; Collins, J.; Lively, R. P.; Schmidt, J. R.; Vasenkov, S. Influence of Hydrogen Sulfide Exposure on the Transport and Structural Properties of the Metal–Organic Framework ZIF-8. *J. Phys. Chem. C* **2018**, *122* (13), 7278–7287.
- (41) Zhang, H.; Liu, D.; Yao, Y.; Zhang, B.; Lin, Y. S. Stability of ZIF-8 Membranes and Crystalline Powders in Water at Room Temperature. *J. Memb. Sci.* **2015**, *485*, 103–111.
- (42) Tian, F.; Cerro, A. M.; Mosier, A. M.; Wayment-Steele, H. K.; Shine, R. S.; Park, A.; Webster, E. R.; Johnson, L. E.; Johal, M. S.; Benz, L. Surface and Stability Characterization of a Nanoporous ZIF-8 Thin Film. *J. Phys. Chem. C* **2014**, *118* (26), 14449–14456.
- (43) Zhang, W.; Hu, Y.; Ge, J.; Jiang, H.; Yu, S.; Zhang, W.; Hu, Y.; Ge, J.; Jiang, H.; Yu, S. A Facile and General Coating Approach to Moisture / Water- Resistant Metal-Organic Frameworks with Intact Porosity A Facile and General Coating Approach to Moisture / Water- Resistant Metal-Organic Frameworks with Intact Porosity. *J Am Chem Soc* **2014**, *136*, 16978–16981.
- (44) Park, K. S.; Ni, Z.; Cote, A. P.; Choi, J. Y.; Huang, R.; Uribe-Romo, F. J.; Chae, H. K.; O’Keeffe, M.; Yaghi, O. M. Exceptional Chemical and Thermal Stability of Zeolitic Imidazolate Frameworks. *Proc. Natl. Acad. Sci.* **2006**, *103* (27), 10186–10191.
- (45) Kizzie, A. C.; Wong-foy, A. G.; Matzger, A. J. Effect of Humidity on the Performance of Microporous Coordination Polymers as Adsorbents for CO<sub>2</sub> Capture. *Langmuir* **2011**, *27* (10), 6368–6373.
- (46) Knoll, W. Interfaces and Thin Films as seen by bound Electromagnetic Waves. *Annu. Rev. Phys. Chem.* **1998**, *49* (1), 569–638.
- (47) Ma, B. H.; Jen, A. K.; Dalton, L. R. Polymer-Based Optical Waveguides : Materials , Processing , and Devices. *Adv. Mater.* **2002**, *19*, 1339–1365.
- (48) Hang, K.; Lau, A.; Tan, L.; Tamada, K.; Sander, M. S.; Knoll, W. Highly Sensitive Detection of Processes Occurring Inside Nanoporous Anodic Alumina Templates : A Waveguide Optical Study. *J. Phys. Chem. B* **2004**, *108*(30), 10812–10818.
- (49) Cameron, P. J.; Jenkins, a. T. a.; Knoll, W.; Marken, F.; Milsom, E. V.; Williams, T. L. Optical Waveguide Spectroscopy Study of the Transport and Binding of Cytochrome c in

- Mesoporous Titanium Dioxide Electrodes. *J. Mater. Chem.* **2008**, *18* (36), 4304.
- (50) Kim, D. H.; Lau, K. H. A.; Robertson, J. W. F.; Lee, O.-J. J.; Jeong, U.; Lee, J. I.; Hawker, C. J.; Russell, T. P.; Kim, J. K.; Knoll, W. Thin Films of Block Copolymers as Planar Optical Waveguides. *Adv. Mater.* **2005**, *17* (20), 2442–2446.
- (51) Kim, D. H.; Lau, K. H. A.; Joo, W.; Peng, J.; Jeong, U.; Hawker, C. J.; Kim, J. K.; Russell, T. P.; Knoll, W. An Optical Waveguide Study on the Nanopore Formation in Block Copolymer/Homopolymer Thin Films by Selective Solvent Swelling. *J. Phys. Chem. B* **2006**, *110* (31), 15381–15388.
- (52) Hang, K.; Lau, A.; Knoll, W. Theoretical Optical Waveguide Investigation of Self-Organized Polymer Thin Film Nanostructures with Nanoparticle Incorporation Optical Waveguide Spectroscopy. *Macromolecular research* **2007**, *15*(3), 211-215.
- (53) Yang, X.; Lin, X.; Zhao, Y.; Zhao, Y. S.; Yan, D. Lanthanide Metal-Organic Framework Microrods: Colored Optical Waveguides and Chiral Polarized Emission. *Angew. Chemie Int. Ed.* **2017**, *56* (27), 7853–7857.
- (54) Ma, H.; Jen, A. K.-Y.; Dalton, L. R.; Ma, B. H.; Jen, A. K.-Y.; Dalton, L. R. Polymer-Based Optical Waveguides: Materials, Processing, and Devices. *Adv. Mater.* **2002**, *19*, 1339–1365.
- (55) Shekhah, O.; Liu, J.; Fischer, R. A.; Wöll, C. MOF Thin Films: Existing and Future Applications. *Chem. Soc. Rev.* **2011**, *40* (2), 1081.
- (56) Hou, C.; Xu, Q.; Peng, J.; Ji, Z.; Hu, X. (110)-Oriented ZIF-8 Thin Films on ITO with Controllable Thickness. *ChemPhysChem* **2013**, *14* (1), 140–144.
- (57) Zimpel, A.; Preiß, T.; Röder, R.; Engelke, H.; Ingrisich, M.; Peller, M.; Rädler, J. O.; Wagner, E.; Bein, T.; Lächelt, U.; Wuttke, S. Imparting Functionality to MOF Nanoparticles by External Surface Selective Covalent Attachment of Polymers. *Chem. Mater.* **2016**, *28* (10), 3318–3326.
- (58) Tan, J.; Bennett, T. D.; Cheetham, A. K. Chemical Structure, Network Topology, and Porosity Effects on the Mechanical Properties of Zeolitic Imidazolate Frameworks. *Proc. Natl. Acad. Sci. U. S. A.* **2010**, *107* (22), 9938–9943.
- (59) Tuninetti, J. S.; Rafti, M.; Azzaroni, O. Early Stages of ZIF-8 Film Growth: The Enhancement Effect of Primers Exposing Sulfonate Groups as Surface-Confined Nucleation Agents. *RSC Adv.* **2015**, *5* (90), 73958–73962.
- (60) Rafti, M.; Allegretto, J. A.; Segovia, G. M.; Tuninetti, J. S.; Giussi, J. M.; Bindini, E.; Azzaroni, O. Metal–organic Frameworks Meet Polymer Brushes: Enhanced Crystalline Film Growth Induced by Macromolecular Primers. *Mater. Chem. Front.* **2017**, *1*(11), 2256-2260.
- (61) Wang, H.; Jian, M.; Qi, Z.; Li, Y.; Liu, R.; Qu, J.; Zhang, X. Specific Anion Effects on the Stability of Zeolitic Imidazolate Framework-8 in Aqueous Solution. *Microporous Mesoporous Mater.* **2018**, *259*, 171–177.

- 1  
2  
3 (62) Zhang, L.; Hu, Y. H. Strong Effects of Higher-Valent Cations on the Structure of the  
4 Zeolitic Zn(2-Methylimidazole)<sub>2</sub> Framework (ZIF-8). *J. Phys. Chem. C* **2011**, *115* (16),  
5 7967–7971.  
6  
7  
8  
9  
10  
11  
12  
13  
14  
15  
16  
17  
18  
19  
20  
21  
22  
23  
24  
25  
26  
27  
28  
29  
30  
31  
32  
33  
34  
35  
36  
37  
38  
39  
40  
41  
42  
43  
44  
45  
46  
47  
48  
49  
50  
51  
52  
53  
54  
55  
56  
57  
58  
59  
60

TOC Graphic



1  
2  
3  
4  
5  
6  
7  
8  
9  
10  
11  
12  
13  
14  
15  
16  
17  
18  
19  
20  
21  
22  
23  
24  
25  
26  
27  
28  
29  
30  
31  
32  
33  
34  
35  
36  
37  
38  
39  
40  
41  
42  
43  
44  
45  
46  
47  
48  
49  
50  
51  
52  
53  
54  
55  
56  
57  
58  
59  
60